MJFAS MALAYSIAN JOURNAL OF FUNDAMENTAL AND APPLIED SCIENCES
PRINT ISSN: 2289-5981 | ONLINE ISSN: 2289-599X

RESEARCH ARTICLE

Flood monitoring and forecasting using synthetic aperture radar (SAR) and meteorological data: A case study

Md Mafijul Islam Bhuiyan [a], SNM Azizul Hoque [b,*]

[a] *Department of Physics, University of Alberta, Edmonton, T6G 2E9, Alberta, Canada*
[b] *Department of Physical Sciences, School of Engineering and Computer Sciences, Independent University, Bangladesh (IUB), Dhaka, Bangladesh*

* *Corresponding author: ahoque@iub.edu.bd*

Article history
Received 16 May 2019
Revised 28 August 2019
Accepted 3 October 2019
Published Online 15 June 2020

Abstract

Availability of several space-borne synthetic aperture radar (SAR) missions has widened the scope of utilizing radar images for monitoring flooded areas. In this paper, the capability of SAR data was investigated to assess and map flooded regions in Sylhet, located in the northeast part of Bangladesh. Co-polarized (VV) Satellite imageries from 2017 have been collected from Sentinel-1A and Sentinel-1B to use in this study. Relative Humidity (RH), Soil moisture and the amount of precipitation data have been used to predict spatiotemporal inundation in Sylhet region. Digital Elevation Model (DEM) was implemented to forecast the runoff directions of water from mountain after heavy rainfalls in Sylhet region. Results of this study indicated that temporal flood prediction errors could be minimized especially for shorter lead times and overall, they showed the applicability of SAR which in combination with images from SAR, DEM and meteorological data that could be exploited to monitor the flooded areas and give better forecasts.

Keywords: GEOINT, Flood forecasting, flood monitoring, sentinel-1, DEM, meteoroidal data

INTRODUCTION

Bangladesh is a developing country where the largest employment sector is agriculture. The country is predominately a rich fertile flat land where most parts are less than 12m above sea level. Its ecology includes a long sea coastline, numerous rivers and tributaries, lakes, different types of forests (i.e., 17% of the country) and flat land with tall grass. Most parts of the rural areas are affected by natural and human-made calamities such as floods, riverbank and embankment erosion, deforestation etc. Every year natural disasters cause havoc where thousands of people are died, millions of them are made homeless, lands and roads are damaged. A GEOINT system based on satellite imageries can be successfully modelled to reduce or even avoid the devastating effects of these calamities.

GEOINT (GEOspatial INTelligence) can be defined as the exploitation or analysis of imageries and geospatial information that explains, quantifies, and visually depicts physical features and geographically referenced activities on the Earth surface due to anthropogenic and natural causes (State of GEOINT Report, 2016; Baber, 2018). GEOINT enables decision makers to take immediate action as well as prepare strategic plans. It encompasses three components, imagery, imagery intelligence and geospatial information (Murdock and Clark, 2016). Geospatial Information is the value-added product derived from geospatial data through human or machine processing. Such data or imagery is generally acquired from satellites, Unmanned Arial Vehicles (UAV), GPS waypoints etc. In this study, freely available imageries from Earth Observation Satellites such as Sentinel-1 launched by the European Space Agency (ESA) (Sentinel-1 2017) were used.

Satellite imageries of a flood affected area in Sylhet division, Bangladesh were collected and processed to develop a GEOINT system. This system is enable to monitor the flooded areas and ϖ estimate the surface areas of the inundated zones. The endeavour will thus help policy makers to identify severely affected areas where relief operations for flood victims need boosting.

Although floods can be monitored using a telemetered network by deploying over large areas (Marín-Pérez *et al.* 2012), use of the technique is declining (Vörösmarty *et al*., 2001). Weather satellite and GPS are used in a wide variety of applications (Hoque *et al.* 2019, Manu *et al.* 2019, Hoque and Fenrich, 2018; Hoque and Ahmed, 2016, Hoque, 2016). Recently, several satellite-based flood forecast models have been proposed (Mason et al. 2014; Hostache et al. 2010; Biancamaria et al. 2011; Pintado et al. 2015). Using satellite-based water level observations (WLOs) Hostache et al. and Biancamaria et al. proposed a flood forecasting model for a river network. However, there are errors in the discharge of water into that modelled area. This is because of the height of the water levels, water discharge and the estimation of the model parameters are inter-related. Pintado et al. overcame these problems by estimating water inflow with uncertainties. However, his forecast model needs to be improved for faster flow of water and steeper rivers.

SAR data has been used to map and monitor flood (Brivio et al., 2002; Gan et al., 2012). Flood monitoring and mapping in India and Bangladesh due to monsoon rain are studied using SAR data collected from RADARSAT satellites (Rahman and Thakur, 2018; Dewan *et al*., 2006). The SAR data from RADARSAT satellite is not freely available while SAR data from the Sentinel-1 is freely available. In this study, SAR data was collected from Sentinel-1.

DATA COLLECTION

Satellite images for the area of interest (AOI) were freely available on ESA's website. Fig. 1 shows the AOI (box filled with red color) in google map.

Sylhet division was our area of interest (AOI). All the images were collected for this area but with different acquisition dates. The corner coordinates (i.e., longitudes and latitudes) of the AOI were NW (90.93, 25.24), NE (92.29, 25.24), SE (92.29, 24.06), and SW (90.93, 24.06). These images were Ground Range Detected (GRD) type and acquisition mode was Interferometric Wide-Swath (IW). Co-polarized (i.e., VV) images have less thermal and ambient noises. Other than the first acquisition (March 14, 2017), the imageries of the same acquisition area were obtained at 12 days interval. These satellite images were from May 25, 2017 to September 22, 2017 and were collected from Sentinel -1. The Sentinel-1A and-1B satellites were launched in April 2014 and April 2016, respectively. Sentinel-1 can process multi-look SAR images available to the user in only an hour after being downloaded to the ground station (Boni et al. 2016). The SNAP desktop application was then used to process acquired satellite imageries.

Fig. 1 (a) Area of Interest (red square) and the location of Bangladesh (b) The area of interest for monitoring and forecasting flood.

METHODOLOGIES

Forecasting of flood using meteorological data and Digital Elevation Model (DEM)

In this study, meteorological data and DEM have also been exploited to predict spatiotemporal inundation in Sylhet regions. DEM data was retrieved from Shuttle Radar Topography Mission (SRTM) (DEM 2018). The resolution of data was 1 Arc-Second. This DEM data would provide the elevation of each coordinate (i.e., the longitudes and latitudes) in meters with 30 m spatial resolution. We used this resolution since high-resolution (i.e., 1 m) DEM data from TANDEM-X radar was not available for our AOI. DEM data is crucial for forecasting potential flooded regions. It can provide the runoff directions of mountain torrents following heavy rainfalls which is important since mountain torrents generally cause flash floods.

Meteorological data, such as Relative Humidity (RH), Soil Moisture, and precipitation amount over a specified period, was taken into account to forecast flood areas and times in the Sylhet region. Meteorological data was collected for the period March 14, 2017 to September 10, 2017 at one-minute time intervals. Data was gathered from the Bangladesh Meteorological Department (BMD) website (BMD 2018). The BMD weather station is in Sylhet (24°53'58.37"N, 91°53'7.09"E). The soil moisture data for the area of interest (AOI) was acquired by the surface soil moisture sensors (Paul 2014). Since 1979, BMD has accumulated soil moisture data in its archive for four different depths: soil layer-1 (0-7cm), soil layer-2 (7-28cm), soil layer-3 (28-100cm), and soil layer-4 (100-255cm). In this paper, the average soil moisture data was considered from the surface layer (0-7cm) (Paul 2014; Mondol et al. 2017). The soil moisture of the surface layer (0-7cm) is highly correlated with relative humidity and temperature during the wet season (Paul 2014). The total amount of precipitation is one of the critical parameters for developing a flood forecasting model and this parameter has a strong correlation with the percentage of soil moisture. Temporal flood prediction errors can be minimized, especially for shorter lead times, and imminent floods can be forecasted efficiently using soil moisture data. The impact of soil moisture on the severity of floods is as follows: higher soil moisture conditions preceding an extreme rainfall event will lead to massive amounts of runoff and, consequently, to extreme flooding associated with the rainfall events. Recent studies of climate change projections (Gutowski *et al.*, 2004; Pan *et al.*, 2001) have been suggested that summer precipitation strongly depends on surface processes, like soil moisture and evapotranspiration (Randall et al. 2010). However, the potential impact of soil moisture on extreme rainfall events has been less often as a scientific focus until now.

In this study, statistical analysis of precipitation amount, relative humidity, and soil moisture was performed. Running average values of the time series of these three parameters were computed over the period from March 14, 2017 to September 10, 2017. Our intention was to calibrate a model based on rainfall data collected during the period with one-minute temporal resolution in Sylhet [24°53'58.37"N, 91°53'7.09"E]. Subsequently, we computed cumulative rainfall to investigate heavy precipitation over that period. Identifying heavy rain within a shorter amount of time can help to predict flash flooding particularly, in foothill areas. The following equation was used to compute the running average of the meteorological parameter (i.e., precipitation amount, relative humidity, and soil moisture).

$$P_{ravg} = \frac{\sum_{i}^{\forall i \, \epsilon \, \Delta t} p_i}{N_{\Delta t}} \quad (1)$$

In the above equation, P_{ravg} is the running average of P, $N_{\Delta t}$ is the total number of samples in Δt time, and p_i is the i[th] sample. The following two equations were used to compute the cumulative sum of precipitation.

$$P_{N+1} = \sum_{i=1}^{N} p_i \quad (2)$$

$$P_{cumsum} = [P_1 \, P_2 \, P_3 \ldots \ldots \ldots \, P_N] \quad (3)$$

Flood events were predicted for the specified AOI by combining the statistical analysis of meteorological data and DEM collected from satellite data.

Flood monitoring through satellite imageries

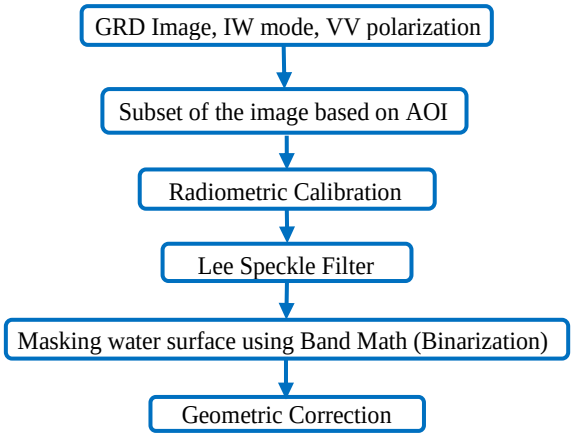

Fig. 2 Schematic diagram of the method of flood monitoring system.

After the acquisition of satellite imageries, different post-processing methods such as radiometric calibration, filtering speckle noise (i.e., Lee filtering), masking of water surface area using band math, and geometric correction were applied to map the flooded regions of Sylhet division. The original satellite images were cropped to a small area of interest to make all subsequent processing steps faster. Furthermore, products of different processing steps also require less storage space if the original images are cropped. The various processing steps are described in Fig. 2.

To proceed, radiometric calibration was applied to generate a new product with calibrated values of the backscatter coefficient so that the pixel values of the SAR images would genuinely represent the radar backscatter of the reflecting surfaces. Sigma Naught calibration was applied to extract water surface areas of an image and compare images that collected at different times. Unlike optical remote sensing images, SAR images are affected by speckle noise. In this study, Lee scalar speckle filtering method with 7 pixels sliding window size was applied (Mascarenhas 1997; Rangaraj *et al*., 1998; Lee *et al*., 2009). Additionally, using Band Math with the threshold value of $2.18 \times 10^{-2}\ dB$ was applied to mask the water surface in order to distinguish from the non-water surface. Following this, geometric terrain corrections were implemented on SAR images to compensate for distortions due to topographical variations of a scene and the tilt of the satellite sensor. The Range Doppler Terrain Correction Operator implements the Range-Doppler orthorectification method (Small et al. 2008) for geocoding SAR images from a single 2D raster radar geometry. In this paper, SRTM3Sec DEM, 10m pixel spacing and WGS84 map projection were considered. The bilinear interpolation method was used for DEM and image resampling. A KMZ file was then generated to visualize the water surface (marked red in Fig. 10 – Fig. 19) in the google earth. The visualized images have been interpreted in the result section.

RESULTS AND DISCUSSION

A running average of precipitation (Fig. 3), relative humidity (Fig. 4), and soil moisture (Fig. 5) for each time window during the interval was computed. Soil moisture on May 25 was elevated, imposing the increase in evaporation rate and eventually raising the average RH to almost 80%. RH was raised due to the precipitation, and this is reflected in Fig. 6. Soil moisture was increased linearly from May 25 to August 05. During this time, RH was remained fluctuating from 84% to 87%. This indicated for higher rainfall in this period, shown in Fig. 6. Average soil moisture was increased considerably from August 5 to September 10. The amount of rainfall was also higher during this time. Therefore, the strong positive correlation among RH, precipitation, and soil moisture was observed during the interval.

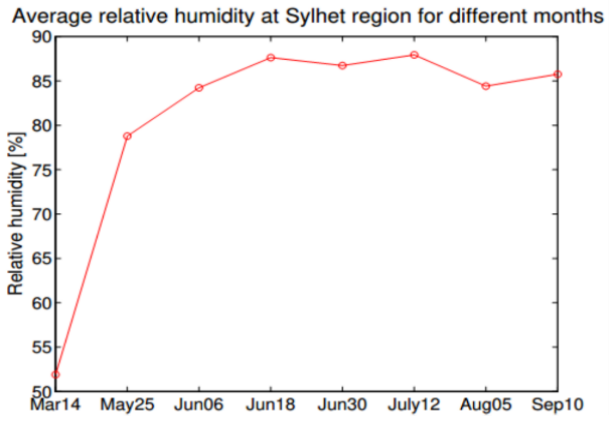

Fig. 3 Average relative humidity for selected months in the Sylhet region.

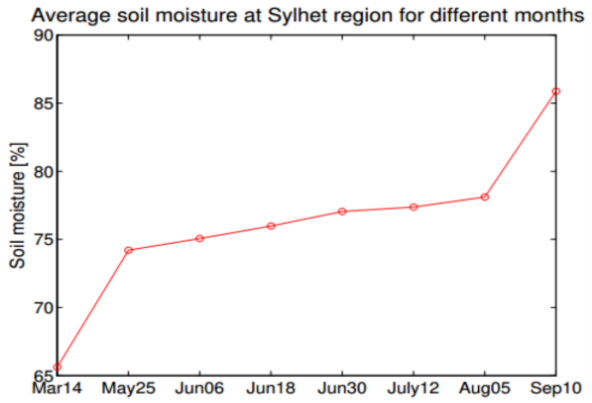

Fig. 4 Average soil moisture for selected months in the Sylhet region.

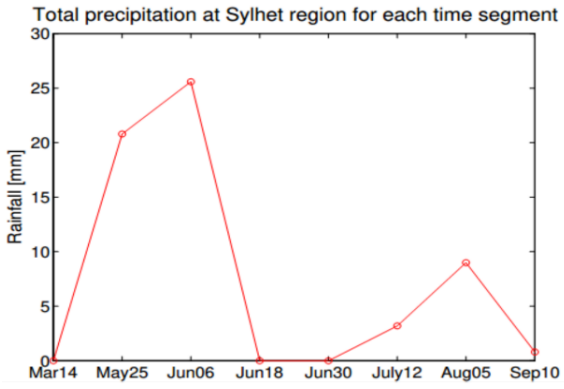

Fig. 5 Average precipitation for selected months in the Sylhet region.

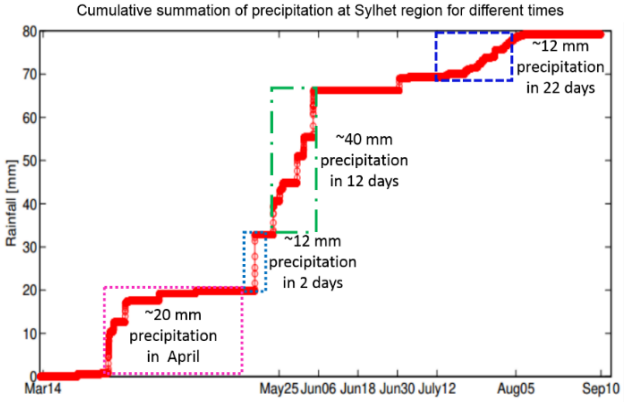

Fig. 6 Cumulative precipitation in the Sylhet region from 14th of March to the 10th of September.

From DEM data, it was observed that Sylhet is located in the foothills of Indian mountainous areas. Fig. 7 depicts the flat DEM data of the AOI. The Indian mountains are located in the north and Sylhet is located in south. The elevation is drastically decreased from 1800m (north) to almost sea level (south). Fig. 8 displays the 3D view of the white rectangular area of Fig. 7. 2D elevations from north to south were plotted and is shown in Fig. 9. It was observed from DEM data that the falling slope was slightly steeper in the south-west direction where Chatak, Sunamgonj, Jagannathpur are located. This indicated that following heavy rainfall, water from upstream would run-off in the low level areas and might cause a flash flood.

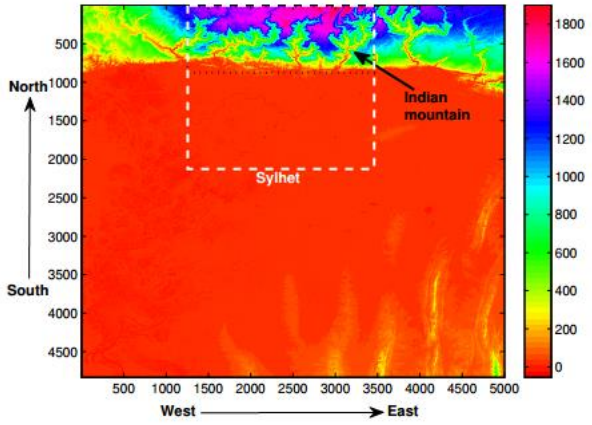

Fig. 7 Flat Digital Elevation Model (DEM) of the AOI. The black dotted line indicates Indian mountainous area with high elevation.

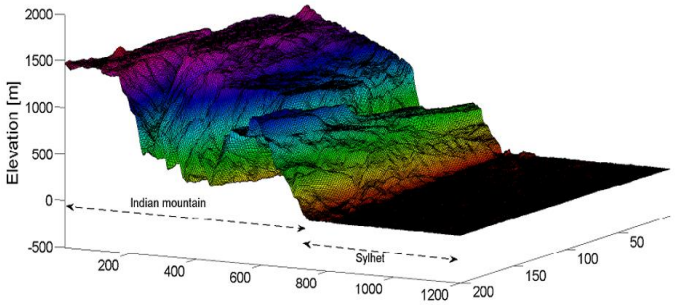

Fig. 8 Three dimensional Digital Elevation Model (DEM) of the white rectangle area of Fig. 7.

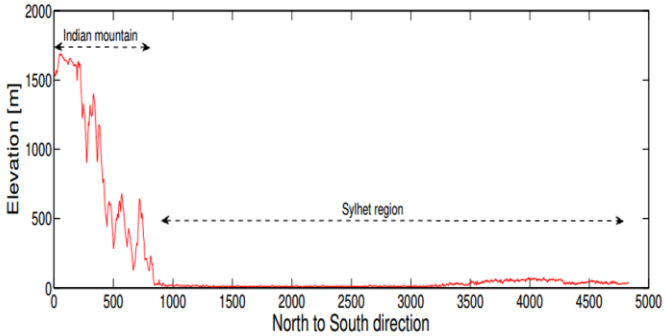

Fig. 9 Two dimensional elevation of Fig 8 (from north to south). The east-west elevation is averaged.

Fig. 6 shows cumulative precipitation from March 14, 2017 to September 10, 2017 in AOI. Almost 20 mm of rainfall was recorded within 20 days in the beginning of April. There was no rain and soil moisture was lower at the time, however, it could be predicted that flash flooding would occur in the south-west of Sylhet due to heavy rainfall within the short amount of time. The orange dotted line in Fig. 10 shows the areas where flash floods were predicted. There was no rain even in the next 15-18 days, however, soil moisture was gradually increased due to flash flood. Subsequently, there was heavy rainfall (~52 mm) from mid of May to June 06. The heavy rainfall was further increased the soil moisture, enabling the prediction of more flash floods in the south-west region of Sylhet. It could also be predicted that fluvial flooding would occur in the northern areas of Sylhet due to the overflow of the river basin. These predicted areas are shown in Fig. 10 using a green dotted line.

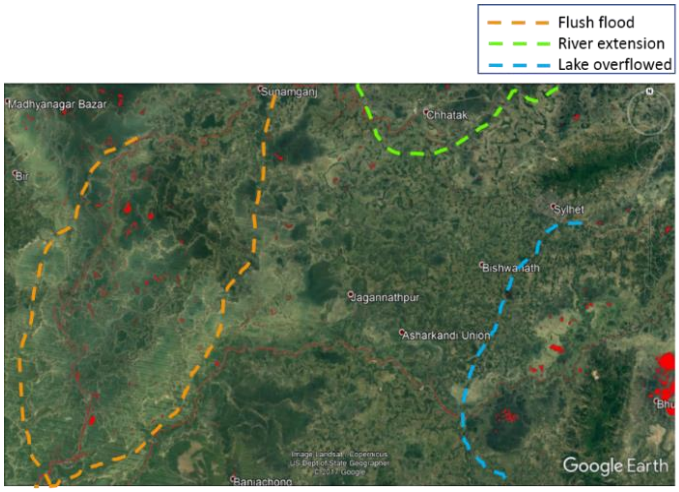

Fig. 10 Prediction of different flooded areas at Sylhet region.

The existing flood water (from May 25, 2017 to September 10, 2017) near Sylhet, [24°53'58.37"N, 91°53'7.09"E] was not discharged properly through the river basin area. Moreover, due to higher soil moisture, flood water did not penetrate in the subsurface. In this scenario, additional rainfall from July 12 to August 05, as shown in Fig. 6 using a blue dotted line, could extend the inundated areas. Therefore, southeast areas of Sylhet were also predicted to be flooded due to this additional precipitation. This region (i.e., Bukshimail Union) is shown in Fig. 10 using a cyan dotted line. In the next section, the predictions will be verified with flood maps generated using SAR imageries.

Fig. 11 Shaded water surface areas (red) on March 14, 2017.

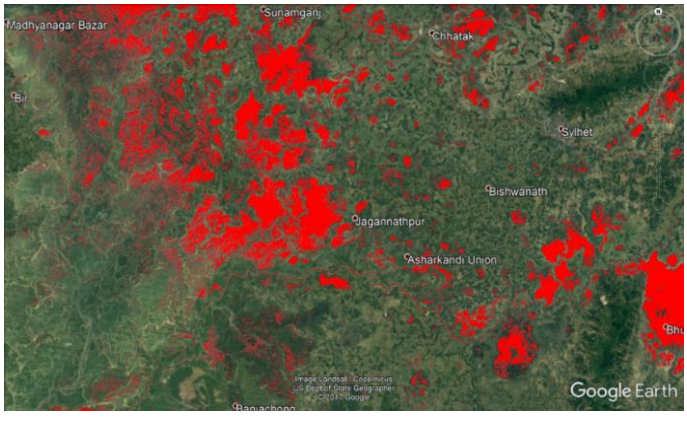

Fig. 12 Shaded water surface areas (red) on May 25, 2017.

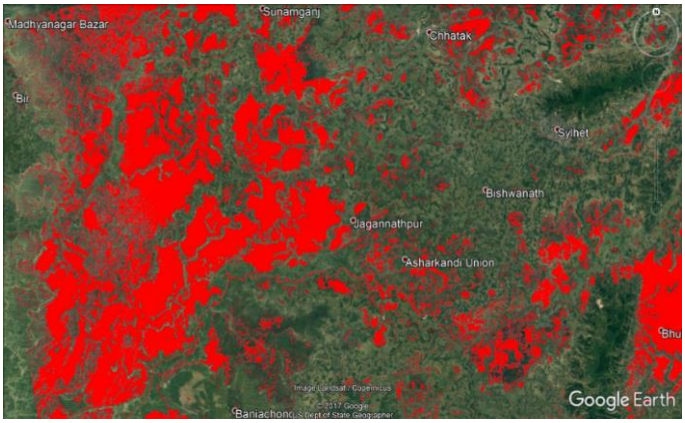

Fig. 13 Shaded water surface areas (red) on June 06, 2017.

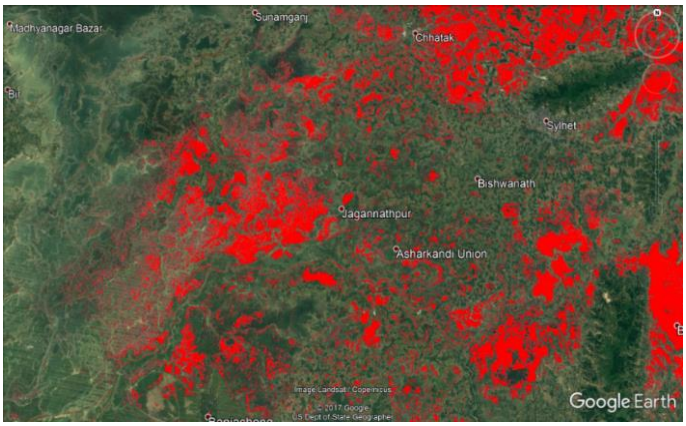

Fig. 14 Shaded water surface areas (red) on June 18, 2017.

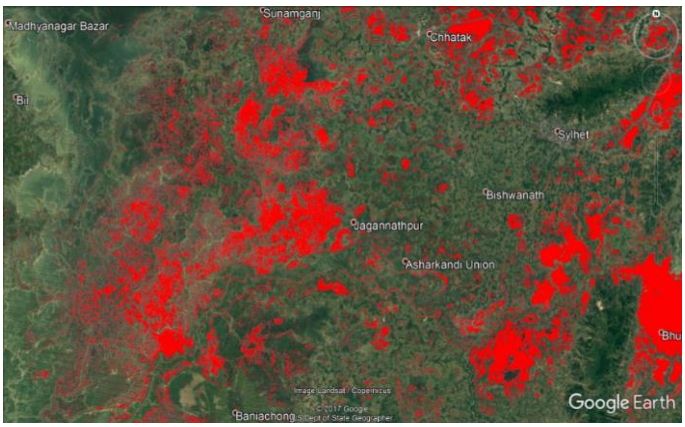

Fig. 15 Shaded water surface areas (red) on June 30, 2017.

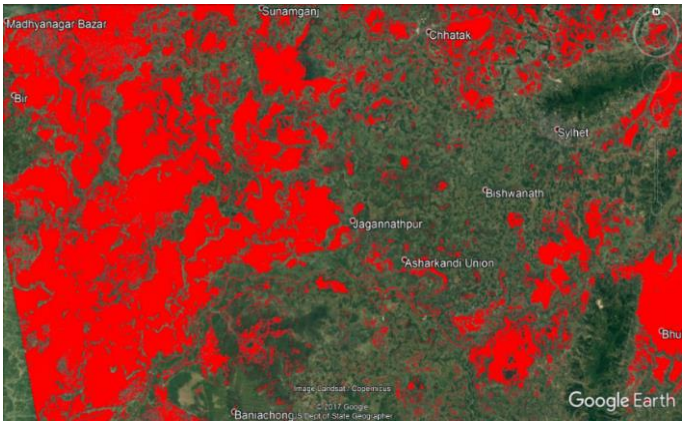

Fig. 16 Shaded water surface areas (red) on July 12, 2017.

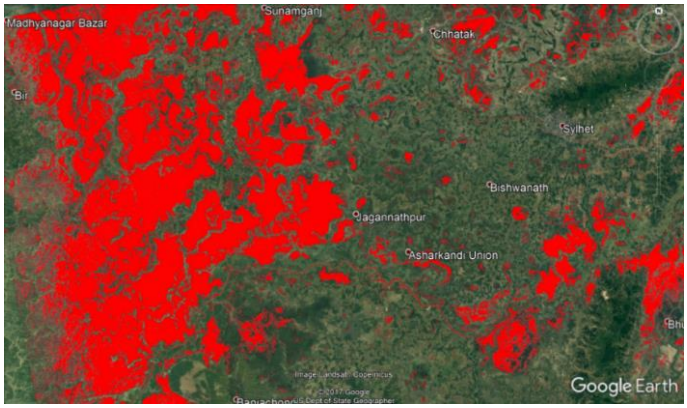

Fig. 17 Shaded water surface areas (red) on August 05, 2017.

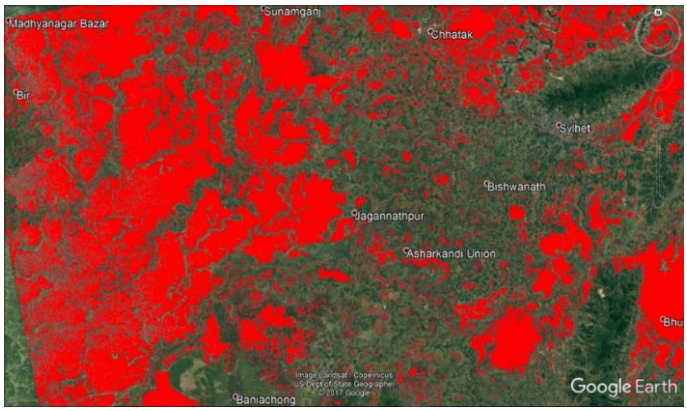

Fig. 18 Shaded water surface areas (red) on September 10, 2017.

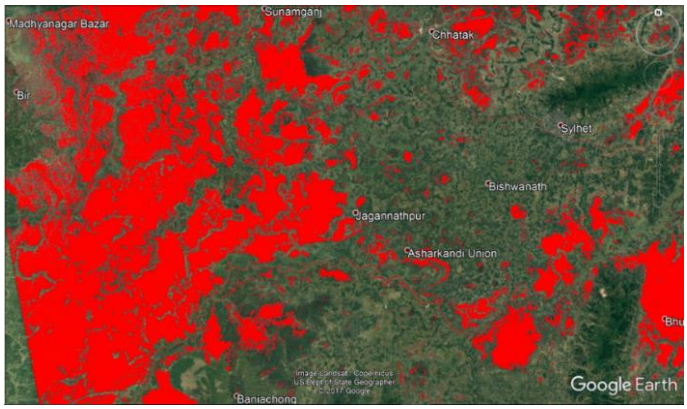

Fig. 19 Shaded water surface areas (red) on September 22, 2017.

As most parts of Sylhet division were heavily inundated this year (i.e., 2017), hence we considered this area as our region of interest (ROI) in this project. Fig. 11 shows that most parts of ROI (i.e., Sylhet division) were dry at the end of the winter season (i.e., March 14, 2017). As predicted, the orange dotted line shown in Fig. 10, some parts of Chhatak, Sunamgonj, and Jagannathpur were flash flooded on May 25, 2017, the beginning of Rainy season (Fig. 12). One can see from Fig. 13 that Sunamgonj district was heavily flooded in the next 12 days (June 06, 2017) due to heavy rainfall and mountain torrents which were also predicted in Fig. 10. By June 30, depicted in Fig. 15, Chhatak was also heavily flooded due to the overflow of the river basin. The flood situation was deteriorated drastically in July 2017 when some parts of the Sylhet urban area were also going underwater (Fig. 16). Fig. 17, 18, and 19 show flooded areas in August and September, respectively. There was no improvement of the flood condition during this period. Instead, it was worsened in Sunamgonj district while most of Chhatak and Sylhet urban areas were under water. On the other hand, from all these figures, it was observed that some parts of Sylhet division were

never or less affected by flood throughout 2017. These areas were Habiganj, Baniachong, and Bishwanath. The reason behind this is that these regions have the highest elevation. DEM data shown in Fig. 13 also supported this assumption. Flood maps also showed that predicted inundated areas were matched with flood maps, however, prediction on timing of flood was not very accurate. Improving this would require the need to find a threshold precipitation and acquire some real-time data of upstream river flow and river water level. Combining this information would improve the accuracy of temporal flood prediction for the AOI.

Table 1 Percentage and size of affected areas

Date	% of water surface area	Water surface area (km^2)
March 14, 2017	0.09	11.88
May 25, 2017	26.93	3554.76
June 06, 2017	28.7	3788.4
June 18, 2017	20.73	2736.36
June 30, 2017	26.23	3462.36
July 12, 2017	35.99	4750.68
July 24, 2017	22.82	3012.24
August 5, 2017	31.8	4197.6
September 10, 2017	35.17	4642.44
September 22, 2017	35.16	4641.12

Table 1 shows the percentage of the affected area and the water surface area in (km^2) during the interval. The dimension of the total area was 13200 km^2. The mean level of the flooded area was 3865.1 km^2 with the standard deviation of 738.8 km^2 during the wet season (from March 25, 2017 to September 22, 2017). From Fig. 20, it can be observed that the flooded area went below the mean level on June 18, 2017 which correlated with the level of precipitation (Fig. 5). The level of flooded area increased due to the rainfall on July 12, 2017 (see Fig. 20 and Fig. 5). Although the level of precipitation decreased, the flooded area was decreased on July 24, 2017 due to the flesh flood from upstream into the low level areas.

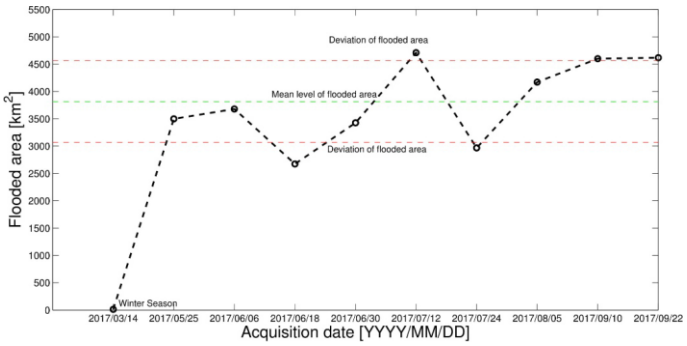

Fig. 20 Areas of the water surface during different temporal baselines.

Conclusions and Future Work

In this study, a statistical method to forecast floods (i.e., flash and fluvial) has been developed using DEM and meteorological data. Satellite imageries were collected of a region of interest (i.e., Sylhet) for the development of a flood monitoring system. Using the prediction model, flash and fluvial flooded areas were forecasted. Then, the model was verified using satellite images. To monitor the extents of the flooded areas, satellite images during different seasons (e.g., winter and rainy seasons) were obtained. The images were processed using a SNAP toolbox (SNAP 2018), image editing software and MATLAB code. Subsequently, processed images were overlaid on Google Earth software for proper visualization. Results showed that during July, August, and September, most parts of Sylhet division, particularly Sunamganj district, were flooded. However, at the end of winter (i.e., March 14, 2017), most parts of Sylhet division were dry, and the areas were started to be inundated at the end of May (i.e., beginning of Rainy season). The depth of water level in the flooded areas could be determined using DEM. All these value-added products would immensely help the relief and disaster management ministry. Currently, the temporal baseline of the collected images was 12 days. In this paper, the forecasting of the flood was retrospective forecasting (hindcasting) rather than real forecasting of the specific area. The Sentinel-1 did not provide near real-time imagery of Bangladesh, although RADARSAT-2 provided almost daily coverage of floods for the European latitudes (Mason et al. 2014). In future, by obtaining images with 6-days or 4-days intervals from any commercial satellite company will make flood monitoring system to be more effective and near-real time.

ACKNOWLEDGEMENT

This work was supported under ICT innovative fund by ICT division, Ministry of Posts, Telecommunications and IT, Government of the People's Republic of Bangladesh. The authors would like to thank Copernicus open access hub for collecting the Sentinel-1 data. DEM data was collected from the Shuttle Radar Topography Mission (SRTM) and the meteorological data was collected from the Bangladesh Meteorological Department (BMD) website. A sincere thanks to Mondar M. M. Ahmed for his diligent work in proofreading this paper and to Choudhury Ben Yamin Siddiqui who developed php code to estimate the area of the flood from the images.

REFERENCES

Baber, M. 2018. *Geospatial Intelligence and National Security. The Geographic Information Science & Technology Body of Knowledge (1st Quarter 2018 Edition)*, John P. Wilson (ed).

Biancamaria, S., Durand, M., Andreadis, K., Bates, P., Boone, A., Mognard, N., Rodríguez, E., Alsdorf, D., Lettenmaier, D., Clark, E. 2011. Assimilation of virtual wide swath altimetry to improve arctic river modeling. *Remote Sensing of Environment*, 115, 373–381.

BMD (2018) http://115.127.34.155:8080/DataLogger/#query. Accessed May 19, 2018.

Boni G., Ferraris L., Pulvirenti L., Squicciarino G., Pierdicca N., Candela L., Pisani A. R., Zoffoli S., Onori R., Proietti C., Pagliara P. (2016) A prototype system for flood monitoring based on flood forecast combined with cosmo-skymed and sentinel-1 data. *IEEE Journal of Selected Topics in Applied Earth Observations and Remote Sensing*, *9*(6), 2794-2805.

Brivio P. A., Colombo R. M., Tomasoni R. 2002. Integration of remote sensing data and GIS for accurate mapping of flooded areas. *International Journal of Remote Sensing*, *23*(2), 429-441.

Dewan A. M., Kankam-Yeboah, K., Nishigaky, M. 2006. Using synthetic aperture radar (SAR) data for mapping river water flooding in an urban landscape: a case study of greater Dhaka, Bangladesh. *Journal of Japan Society of Hydrology and Water Resources*, *19*(1), 44-45

DEM (2018) https://earthexplorer.usgs.gov Accessed May 19, 2018.

Gan T. Y., Zunic, F., Kuo, C. C., Strobl, T. 2012. Flood mapping of Danube river at Romania using single and multi-date ERS2SAR images. *International Journal of Applied Earth Observation*, 18, pp. 69-81.

Gutowski W. J., Otieno F., Arritt R. W., Takle E. S., Pan Z. 2004. Diagnosis and attribution of a seasonal precipitation deficit in a US regional climate simulation. *Journal of Hydrometeorology*, *5*, 230242.

Hoque, S. A., Ahmed, T. 2016. Adapting the NeQuick 2 model to gps derived TEC data at a given location. *AIUB Journal of Science and Engineering (AJSE)*, 15(1), 135-141.

Hoque, S. N. M. A. 2016. Improvement of B2bot correction factor for NeQuick 2 during the high solar activity at Saint Croix. *Journal of Advanced Research Design Volume*, *27*(1), 19-26.

Hoque, S. N. M. A., Fenrich, F. J. 2018. A new technique for understanding magnetosphere-ionosphere coupling using directional derivatives of superdarn convection flow. *Astrophys Astron*, 39: 70.

Hoque, S. N. M., Ahmed, M. M. M., Bhuiyan, M. I. (2019). Investigating rapid deforestation and carbon dioxide release in Bangladesh using geospatial information from remote sensing data. Ecocycles, 5(2), 97-105.

Igor, N., Garkusha, Volodymyr, V., Hnatushenko, Volodymyr, V., Vasyliev. 2017. Using sentinel-1 data for monitoring of soil moisture. *IEEE International Geoscience and Remote Sensing Symposium*, 1656-1659.

Lee J. S., Wen J. H., Ainsworth T. L., Chen K. S., Chen A. J. 2009. Improved sigma filter for speckle filtering of SAR imagery. *IEEE Transactions on Geoscience and Remote Sensing*, *47*(1), 202-213.

Murdock, D., Clark, R. 2016. *Chapter 5 – Geospatial Intelligence" in The Five Disciplines of Intelligence Collection*. Washington DC: CQ Press.

Manu, M. M., Saha, R., Hoque, Snm, Hoque, A. (2019). Remote Environmental Data Analysis Using Sounding Rocket. International Journal of Engineering and Technology. 11. 1209-1221.

Marín-Pérez, R., García-Pintado, J., Skarmeta, A.G. 2012. A real-time measurement system for long-life flood monitoring and warning applications. *Sensors, 12*, 4213–4236.

Mascarenhas N. D. A., edited by Shaun Quegan and Joao R. Moreira. 1997. *An Overview of Speckle Noise Filtering in SAR Images*. Image Processing Techniques, First Latino- American Seminar on Radar Remote Sensing: Proceedings of a conference held 2-4 December 1996, Buenos Aires, Argentina, p.71.

Mason, D., García-Pintado, J., Dance, S., (2014) Improving flood inundation monitoring and modeling using remotely sensed data. in: Civil Engineering Surveyor, pp. 34–37.

Mondol M. A. H., Ara I., Das S. C., (2017) Meteorological Drought Index Mapping in Bangladesh Using Standardized Precipitation Index during 1981–2010, Advances in Meteorology, Volume 2017, Article ID 4642060,

Pan Z., J. H. Christensen, R. W. Arritt, W. J. Gutowski Jr., E. S. Takle and F. Otieno, (2001) Evaluation of uncertainties in regional climate change simulations. J. Geophys. Res. 106, 17735-17751.

Paul M., (2014) Study on long-term soil moisture characteristics over Bangladesh and its relations to atmospheric variables. Masters' Thesis, Bangladesh University of Engineering and Technology (BUET) http://lib.buet.ac.bd:8080/xmlui/handle/123456789/4421.

Pintado J. G., Mason D. C., Dance S. L., Cloke H. L., Neal J. C., Freer J., Bates P. D., (2015) Satellite-supported flood forecasting in river networks: A real case study. Journal of Hydrology, 523, 706-724.

Rahman M. R., Thakur P. K. (2018) Detecting, mapping and analysing of flood water propagation using synthetic aperture radar (SAR) satellite data and GIS: A case study from the Kendrapara District of Orissa State of India. *The Egyptian Journal of Remote Sensing and Space Science*, 21 (1), pp. S37-S41,

Randall, D. A., Wood, R. A., Bony, S., Colman, R., Fichefet, T. and co-authors (2007) Climate models and their evaluation. In: Climate Change 2007: The Physical Science Basis. Contribution of Working Group I to the Fourth Assessment Report of the Intergovernmental Panel on Climate Change, Cambridge University Press, Cambridge, UK

Rangaraj M. Rangayyan, Mihai Ciuc, Farshad Faghih (1998) Adaptive-neighborhood filtering of images corrupted by signal-dependent noise. Appl. Opt. 37, 4477-4487

Sentinel-1 (2017) https://scihub.copernicus.eu/dhus/" Accessed April 01, 2017

Small D., Schubert A. (2008) Guide to ASAR Geocoding, RSL-ASAR-GC-AD, Issue 1.0

SNAP (2018) http://step.esa.int/main/download/ version 5.0 accessed January 2018

Vörösmarty, C., Askew, A., Grabs, W., Barry, R.G., Birkett, C., Dell, P., Goodison, B., Hall, A., Jenne, R., Kitaev, L., Landwehr, J., Keeler, M., Leavesley, G., Schaake, J., Strzepek, K., Sundarvel, S.S., Takeuchi, K., Webster, F., Group, T.A.H. (2001) Global water data: a newly endangered species. Eos Trans. AGU 82, 54–58.